Reconfigurable Vector Vortex Beams Using Spoof Surface Plasmon Ring Resonators

Zhen Liao, *Member, IEEE*, Yanziyi Che, Leilei Liu, Bai Cao Pan, Ben Geng Cai, Jia Nan Zhou, Guo Qing Luo, *Senior Member, IEEE*, , and Yongmin Liu

Abstract—In this paper, a spoof surface plasmon (SSP) ring resonator to generate dynamically reconfigurable vortex beams is proposed. According to the phase constant control of the SSP and the harmonic radiation principle, the tunable cylindrical vector vortex beams (VVBs) with different topological charges can be obtained. The tunable system which operates by electronic control would utilize varactors to change the wavenumber of SPP on the ring resonator and realize the reconfigurable VVBs modes at a fixed frequency. All VVBs have excellent orbital angular momentum (OAM) purity (above 90%). Interestingly, the antenna also simultaneously radiates the scalar vortex beams with tunable OAM modes. Both numerical simulations and experimental characterizations confirm the theoretical predictions. Because the designed antenna has the advantages of simple feeding network, easy bias circuit, as well as miniaturization and integration compatibility, we anticipate that the antenna will enable a wide range of applications for future wireless communication and imaging technologies.

Index Terms—Spoof surface plasmon, vector vortex beam, orbital angular momentum

I. INTRODUCTION

IN recent years, vortex beams showing helical wavefront have attracted a lot of attention due to the additional degree of freedom for wave manipulation. The vortex beams carrying OAM has unbounded eigenstates, which can offer great potential for increasing the spectrum efficiency and communication capacity in wireless systems [1]. Most existing researches were devoted to the case of scalar vortex beams, which have spiral phase and uniform polarization (such as linear and circular polarization) [2]. In contrast, the other kind of vortex beams, which possess spatially inhomogeneous polarization (such as radial polarization, and azimuthal polarization) and azimuthally varying phase pattern in transversal plane, are referred to VVBs [3]. In particular, VVBs with both phase singularity and polarization singularity have a broad range of potential applications ranging from high-resolution imaging [4]–[7] to optical manipulation [8]–[10] and communication [11]–[13]. It has also been demonstrated that the VVBs enable a more robust communication channel with longer distance and lower signal-to-noise-ratio compared with the scalar vortex, when they go through a turbulent atmosphere[14].

Various approaches to generate VVBs have been proposed, including liquid crystal q-plates [15], spatial light modulator [16] and spiral phase plates [17]. However, these techniques usually require bulky devices, which increase the system complexity and limit widespread applications in integration. Metasurface provides a very promising method to produce structured beams on a compact platform [18], [19]. For instance, in a bi-layer cascaded metasurface design [20], the first metasurface is employed to generate vortex phase, and the second one is applied to manipulate the vector polarization. Furthermore, a better solution is to design a single metasurface to generate VVBs [21], such as using a single reflective-type metasurface [22]. Similarly, VVBs can also be generated by transmit-arrays in millimeter-wave, utilizing the Berry phase and dynamic phase [23], [24]. In microwave region, some novel vortex beam emitters based on SSP have been designed [25]–[29]. For example, a looped comb-shaped SSP waveguide surrounded by a series of circular patches was reported to obtain VVBs [26], [28]. In [29], SSP ring resonator can emit VVBs with several different OAM modes at different frequencies.

So far, most designs can only generate specific OAM modes with a certain physical structure, in which multi-OAM-mode vortex beams are generated by changing the operating frequency [30] or the input ports [31]. These designs are inconvenient for practical applications of OAM, such as radar

Z. Liao, Y. Che, B. Pan, B. Cai, J. Zhou, and G. Q. Luo are with the Key Laboratory of RF Circuits & System of Ministry of Education, School of Electronics and Information, Hangzhou Dianzi University, Xiasha High Education Zone, Hangzhou, 310018, China. (e-mail: luoguoqing@hdu.edu.cn)

Z. Liao, B. Pan, and B. Cai, are also with the State Key Lab of Millimeter-Waves, Southeast University, Nanjing 211189, China.

L. Liu is with the National and Local Joint Engineering Laboratory of RF Integration, College of Electronic and Optical Engineering, Nanjing University of Posts and Telecommunications, Nanjing, 210003, China. (e-mail: liull@njupt.edu.cn)

Y. Liu is with the Department of Mechanical and Industrial Engineering and the Department of Electrical and Computer Engineering, Northeastern University, Boston, Massachusetts 02115, USA. (e-mail: y.liu@northeastern.edu)

imaging. It is still a challenge to achieve reconfigurable OAM. In radio frequency, the antenna array is an effective method to generate tunable OAM beams, while the main limitation includes complicated feeding network and expensive phase shifters [32], [33]. In order to resolve this problem, some active metasurfaces have been developed to achieve tunable OAM waves [34], [35]. However, they usually require the independent bias of each unit cell, which increases the complexity and cost. Therefore, the dynamical manipulation of OAM of the vortex waves, especially for VVBs, is very challenging.

In this paper, a reconfigurable VVBs antenna based on SSP ring resonator is proposed. Periodic corrugated ring can radiate the first-order harmonic waves, which are cylindrical VVBs. It is shown that accurate and flexible control of SSP phase constant can be achieved by adjusting the capacitance of the varactor diodes. Thus, VVBs with different topological charges can be produced by simply changing the bias voltage. The proposed antenna with reconfigurable VVBs OAM modes of ±1, and 0 at fixed frequency is demonstrated by simulation and measurement results, which have good agreement with the theoretical design. Compared with the conventional array technique and active metasurfaces, our design avoids the complicated feeding network and bias circuits. Considering the miniaturization and integration compatibility of SSP devices, we think that our method provides a new strategy to implement reconfigurable VVBs antennas for microwave wireless communication and radar imaging applications.

II. RECONFIGURABLE SSP STRUCTURE

Fig. 1 depicts the geometrical details of the proposed tunable SSP structure. It consists of an array of comb-like unit cells, varactors, via hole, substrate and ground. The varactors c_v are inserted between the stubs and the metal strip. The stubs are short-circuited by via holes. The period along the length of the strip is denoted by $d = 8$ mm. Moreover, the thickness and relative permittivity of the substrates are 3 mm and $\varepsilon_r = 2.5$, respectively.

The dispersion curve of the unit cell with $c_v = 0.2$ pF and the groove depth $h = 2.94$ mm is numerically simulated. The simulated results are obtained using an eigen-mode solver in CST Microwave Studio. It is noted that eigen-mode solver in CST does not support the lumped elements. The alternative dielectric model can be readily obtained following the procedure mentioned in [36]. In Fig. 1(b), the dispersion curve has a deviation from the light cone and approaches the asymptotic frequency at 5 GHz, which is similar to natural surface plasmon polaritons in the optical region [37].

To understand the operating principle of the proposed SSP structure, an equivalent circuit model is established, as seen in Fig. 1(c). This equivalent circuit model can be considered as a cascade of a transmission line section of length $d/2$, a shunt short-circuited stub, and another transmission line section of length $d/2$. Furthermore, the short-circuited stub of length h and width a is replaced with an inductor L, while the total distributed parameter effects and the varactor are replaced with

a capacitor C, as shown in Fig. (d). Here, the inductor L can be expressed as

$$L = Z_s tan\theta_s/\omega \qquad (1)$$

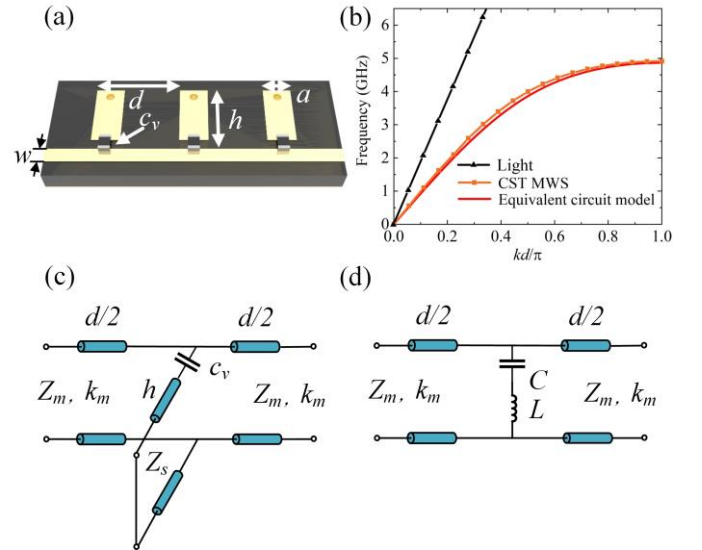where $\theta_s = k_s h$ is the equivalent electric length of the shunt

Fig. 1 (a) Schematic of the reconfigurable SSP structure; (b) Comparison of the dispersion curves of the designed structure from full-wave simulation and the equivalent circuit model; (c) Equivalent circuit model of the proposed structure; (d) Equivalent circuit model of the transmission line loaded with shunt LC-circuit.

stub, k_s represents the propagation constant of the stub, h is the physical length of the stub, and Z_s is the impedance of the stub.

Therefore, the transfer matrix of the nth unit cell is

$$\begin{bmatrix} A & B \\ C & D \end{bmatrix} = \begin{bmatrix} cos\frac{\theta}{2} & jsin\frac{\theta}{2} \\ jsin\frac{\theta}{2} & cos\frac{\theta}{2} \end{bmatrix} \begin{bmatrix} 1 & 0 \\ jY & 1 \end{bmatrix} \begin{bmatrix} cos\frac{\theta}{2} & jsin\frac{\theta}{2} \\ jsin\frac{\theta}{2} & cos\frac{\theta}{2} \end{bmatrix} \qquad (2)$$

where $\theta = k_m d$, k_m is the propagation constant of the unloaded metal strip with width $w = 1$ mm, and Y is the shunt susceptance. According to the descriptions in [38], the value of the shunt capacitance $C = 0.31$ pF can be readily obtained, when the capacitance of varactor is 0.2 pF. Since we mainly focus on the operating principle of the antenna, we do not repeat details here for simplicity.

For the periodically loaded line, we can deduce the dispersion from [39]

$$\begin{vmatrix} A - e^{-jkd} & B \\ C & D - e^{-jkd} \end{vmatrix} = 0 \qquad (3)$$

It can be simplified as

$$cos(kd) = cos(k_m d) + \frac{jZ_m Y}{2} sin(k_m d) \qquad (4)$$

where k is the phase constant of SSPs on the comb-like strip, and Z_m is the impedance of the unloaded line. Fig. 1(b) plots the dispersion curves obtained from CST MWS and those calculated from (3), which show excellent agreement.

From the equivalent circuit model, we can find the dispersion is relevant to Y, indicating L and C. Here, L depends on the length h and width a of the stub, while C is mainly affected by varactor c_v. To verify our prediction, the dispersion curves of the unit cell with different h and c_v are simulated and plotted in Fig. 2. It is apparent that the SSP

exhibit different propagating constants k as h and c_v varies. In this way, we can adjust the wavevector of SSPs by tuning the varactor capacitances c_v and the length of the short-circuited stub h.
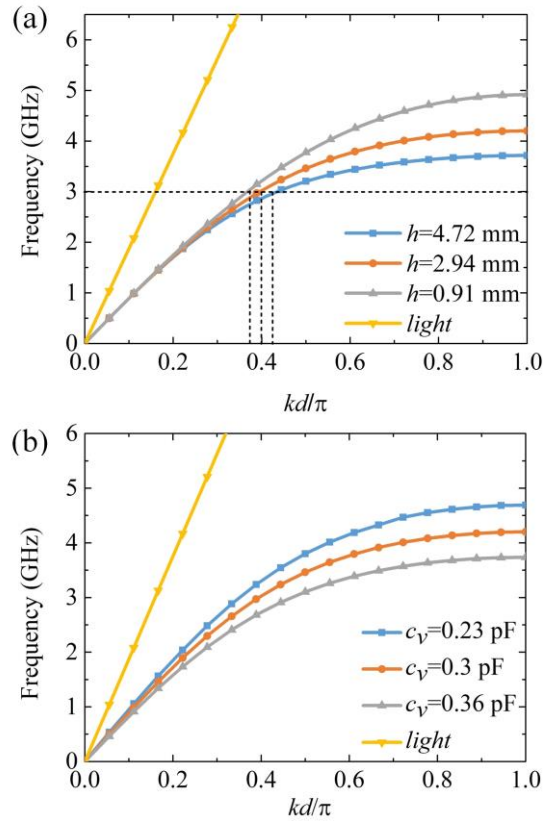

Fig. 2 Simulated dispersion curves of the reconfigurable SSP unit cell with (a) different length h when $c_v = 0.3$ pF and (b) different varactor values c_v when $h = 2.94$ mm. The geometric parameters of the structure are as follows: $d = 8$ mm, $a = 1$ mm.

III. ANTENNA CONFIGURATION DESIGN AND MECHANISM

A. Configuration of Antenna

The proposed dynamic tunable VVBs antenna is designed based on SSP, as shown in Fig. 3. The SSP ring resonator and the metallic comb-like transmission line are etched on FR4 substrate ($\varepsilon_r = 2.5$) with thickness of 3 mm. The ground plane is printed on the lower FR4 substrate layer.

From Fig. 2, we found that periodic corrugated structures support SSP propagation. The phase velocity of SSP is slower than the light in free space, indicating that SSP are confined in a subwavelength scale. The phase velocity of SSP is slower than the light in free space, indicating that SSP are confined in a subwavelength scale. When this SSP waveguide possesses a surface impedance modulated periodically in the SSP propagation direction, the modulated SSP produces higher order modes. If the modulation period is larger than some critical value, one or more higher order modes will radiate away from surface at some angle [40], [41]. The periodic variation of stub lengths is considered as a discrete realization of the continuously varying surface impedance. To realize the electromagnetic radiation, the Fig. 3 presents that the perimeter of the ring contains 10 periods, each of which has five stubs of

unequal length. In this case, the surface impedances in one period follow the triangular distribution, which can be written as

$$Z_s = \begin{cases} jX_s(1 + \frac{2M}{p}x - \frac{M}{2}) & if \ 0 \le x \le \frac{p}{2} \\ jX_s(1 - \frac{2M}{p}x + \frac{3M}{2}) & if \ \frac{p}{2} \le x \le p \end{cases} \quad (5)$$

where X_S is the average surface reactance, and M is the modulation depth, and $x = \varphi R$ is arc length.

After the periodical modulation, the ring resonator can radiate the first-order harmonic wave in azimuthal direction [42], whose wavenumber is:
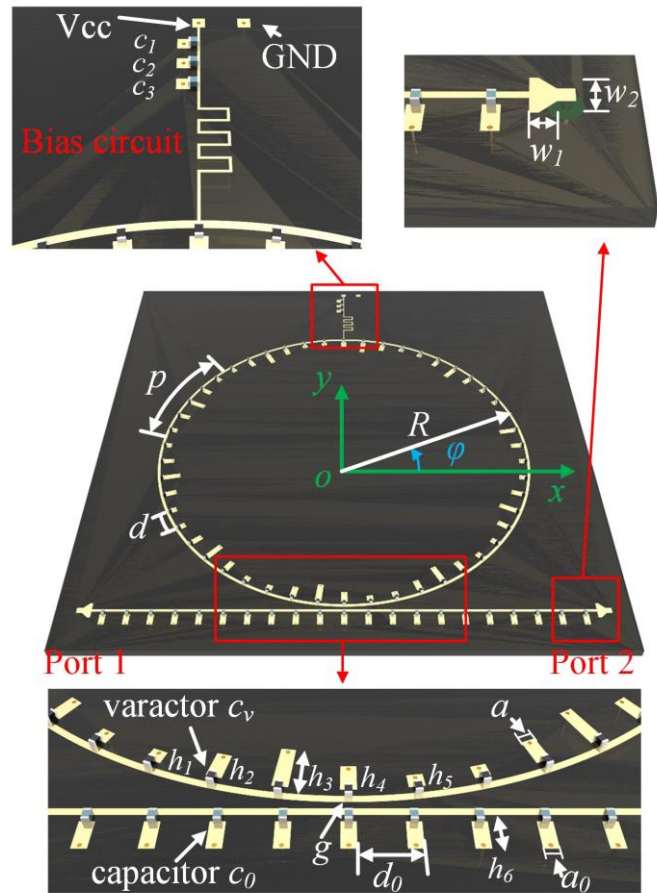

Fig. 3 Geometry of the proposed SSPs ring resonator antenna that is coupled to an access waveguide. (Physical dimensions: $p = 40$ mm, $d = 8$ mm, $a = 1$ mm, $R = 68.4$ mm; $h_1 = 0.91$ mm, $h_2 = 2.94$ mm, $h_3 = 4.72$ mm, $h_4 = 2.94$ mm, $h_5 = 0.91$ mm, $h_6 = 2.94$ mm, $g = 0.2$ mm, $c_0 = 0.3$ µF, $c_1 = 1$ µF, $c_2 = 6.8$ µF, and $c_3 = 2.2$ µF, $d_0 = 8$ mm, $a_0 = 1$ mm, $w_1 = 2$ mm, $w_2 = 5.6$ mm.)

$$k_{\varphi,-1} = k_{\varphi,a} - \frac{2\pi}{p} \quad (6)$$

where $k_{\varphi,a}$ is the average phase constant of SSP on the ring. Hence, the angle of the emitted beam can be calculated as $\arcsin(k_{\varphi,-1}/k_0)$, where k_0 is the vacuum wavenumber.

As a specific example, we design a radiation wave in the vertical direction ($k_{\varphi,-1} = 0$) at 3 GHz, indicating that the average wave number of SSP on the comb-like ring should be $k_{\varphi,a} = 2\pi/p$. Then the average surface reactance can be obtained $Xs = 863$ Ω through:

$$Z = \eta_0 \sqrt{1 - (k_\varphi/k_0)^2} \quad (7)$$

where η_0 is the impedance of free space. Furthermore, we

choose $M = 0.06$ to design the surface impedance distribution. Then the surface impedances of unit cells in one period are 811 Ω, 863 Ω, 915 Ω, 863 Ω, and 811 Ω, respectively. Substituting these results into Eq. (7), we can solve the corresponding $k_\varphi d$ are 0.38π, 0.4π, 0.42π, 0.4π, and 0.38π, respectively. Since the radius R is much bigger than the stubs, the stubs in a very small arc can be seen as in a straight line. Therefore, the propagation constant k_φ in the azimuthal direction is nearly equal to the wavenumber in a straight comb-like strip. As indicated by dashed lines in Fig. 2(a), the final lengths of stubs are chosen as 0.91 mm, 2.94 mm, 4.72 mm, 2.94 mm, and 0.91 mm, with varactor capacitance $c_v = 0.3$ pF, respectively, corresponding to the wavenumber of 0.38π, 0.4π, 0.42π, 0.4π, and 0.38π.

As shown in the bottom inset of Fig. 3, the driven antenna is implemented by a straight comb-like strip near the ring resonator. We set their stubs in with fixed-length equal to $h_6 = 2.94$ mm and capacitor $c_0 = 0.3$ pF, which is the average value of the ring. After that, the SSP on the ring and the feeding strip has similar wavenumbers. In this case, phase- and mode-matched power exchange between the SSP wave on ring resonator and feeding straight strip. For efficient energy exchange, the distance between them is set as $g = 0.2\ mm$. In order to feed the straight comb-like strip, we design a transition between the terminal and the coaxial feeding (see the top right inset of Fig.3).

The bias circuit is depicted schematically in the top left inset of Fig. 3. Dynamic manipulation of the varactor in the ring can be achieved by tuning the voltage between the two solder pads. The low-pass filter technique uses a meander line inductor connected in parallel with three capacitors of $c_1 = 1\mu F$, $c_2 = 6.8\mu F$, and $c_3 = 2.2\mu F$, which prevents the high frequency signals flowing into the direct current (DC) voltage source.

B. Operating Principle of the Antenna

In our design, the whispering gallery resonance occurs when the SSP wave propagate azimuthally around the ring and the optical path in a circumnavigation is equal to an integer multiple of the wavelength. In this regard, the resonant condition should be:

$$2\pi R \cdot k_{\varphi,a}/k_0 = m\lambda \qquad (8)$$

where m is the number of wavelengths along the whole looped comb-like strip, and λ is the wavelength in the air.

It is worth noting that the whispering gallery modes (WGMs) are travelling wave modes. The periodic modulations of stubs cause the WGMs to radiate continuously along the loop. Importantly, the phase constant of the radiated first-order harmonic wave at resonance frequencies can be obtained by substituting Eq. (8) into Eq. (6), that is

$$k_{\varphi,-1} = \frac{m}{R} - \frac{n}{R} \qquad (9)$$

where n is the number of surface impedance modulated periods in the perimeter of the ring ($n = 10$ in our design). In addition, the azimuthal propagation constant of the harmonic beam, which is the phase shift per unit radian along the loop, can be written as

$$\beta_\varphi = k_{\varphi,-1}R = m - n \qquad (10)$$

Since the polarization of the spatial harmonic wave is along

the length of the loop structure, the radiated wave is mainly azimuthal polarization. If we feed the energy from Port 1, the SSP loop resonator is sequentially excited along the counterclockwise azimuthal direction. Then the emitted wave can be described using

$$E_\varphi = E_0(r,z)e^{-j\beta_\varphi\hat{\varphi}} \qquad (11)$$

where $E_0(r, z)$ is the amplitude of the far field and φ is the cylindrical coordinate. Intuitively, this wave function is similar to the general expression $e^{-jl\hat{\varphi}}$, corresponding to a vortex beam. Hence, our generated radiated harmonic waves carry OAM states, which are cylindrical VVBs. Moreover, the topological charge is $l = \beta_\varphi = m - n$ at the resonance frequency. The topological charge l can be reconfigured by adjusting the azimuthal order of the mode m, which is determined by average propagation constant $k_{\varphi,a}$. Furthermore, the topological charge l and calculated average phase constant $k_{\varphi,a}$ of our design at 3 GHz are deduced and shown in Table I. $k_{\varphi,a}d$ should be 0.36π, 0.4π, and 0.44π, when l is equal to -1, 0 and 1, respectively.

As studied in the previous section, the phase constant of our SSP can be tuned by the varactor capacitances and the length of stubs. To realize reconfigurable vortex beam at a given frequency, we investigate the dispersion mappings of fundamental mode with different varactor capacitances and fixed length $h = 2.94$ mm, as exhibited in Fig. 4. As the stub length is fixed, the varactor capacitances c_v can control the asymptotic frequency. Moreover, it is seen that c_v could be chosen to get specific wavenumber at the fixed frequency. As shown in Fig. 4 (the white line at 3 GHz), the capacitance c_v should be 0.23pF, 0.3pF, and 0.36pF to make the corresponding $k_{\varphi,a}d$ equal to 0.36π, 0.4π, and 0.44π, respectively. In theory, we can get more topological charge if the varactor diode has wider capacitance range. Also note that too large of a phase constant will cause excessive loss, low radiation efficiency and OAM mode distortion.

TABLE I
THE CORRESPONDING PARAMETERS FOR EACH OAM MODE.

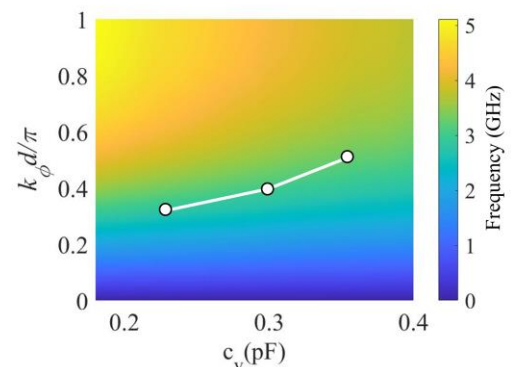| l	-1	0	1
m	9	10	11
$k_{\varphi,a}d$	0.36π	0.4π	0.44π
c_v	0.23 pF	0.3 pF	0.36 pF
Vcc	7.53 V	5.5 V	4.25 V

Fig. 4 Mappings of the wave vector k of the proposed SSP, varying with
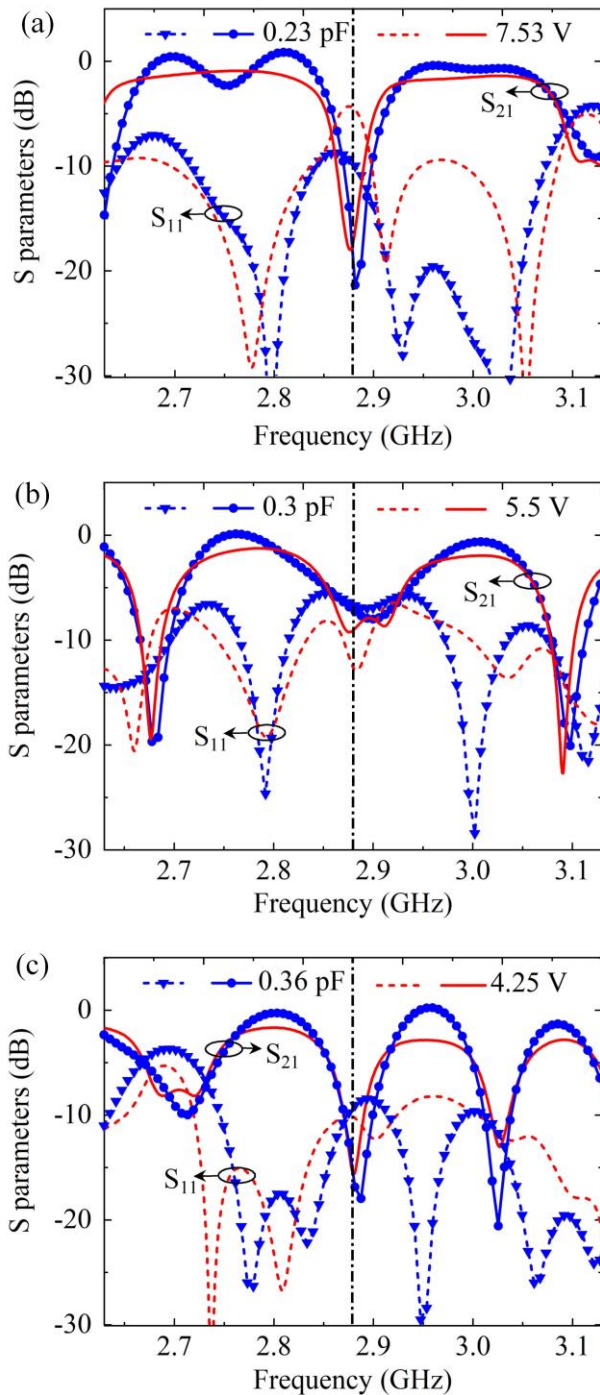
frequency and varactor capacitance c_v.

Fig. 5 Simulated S-parameters of the vortex beams antenna with different varactors and measured S parameters at different bias voltages.
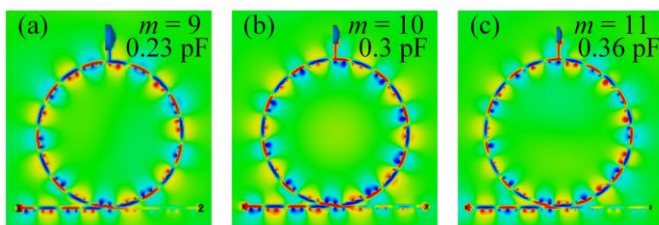

Fig. 6 (a) - (c) indicate the near field with varactor values c_v = 0.23 pF, 0.3 pF, and 0.36 pF, corresponding to mode number m = 9, 10, 11.

IV. PERFORMANCE OF THE PROPOSED ANTENNA

Through the analysis in the previous section, the reconfigurable vortex beam can be obtained in our design. To confirm the performance, the simulated transmission and reflection coefficients are plotted in Fig. 5. It can be seen that S_{21} of proposed antenna has dips at 2.88 GHz when varactor c_v values are equal to 0.23pF, 0.3pF, and 0.36pF. Both the S_{11} coefficients maintain a low level of -10 dB with 0.23 pF, and 0.36 pF. Fig. 5(b) shows that the reflection is higher than -10 dB, stemming from the open stopband (OSB) at broadside radiation. These results demonstrate that the resonances occur at 2.88 GHz, when the varactors are 0.23pF, 0.3pF, and 0.36pF, respectively. According to the parameters given in Section III, a prototype of the proposed loop antenna was fabricated and measured. The type of loaded varactor diode we choose is M46H120. Overall, the experimental results show good agreement with the simulation, when the reverse voltage are 7.53 V, 5.5 V, and 4.25 V. It is noting that there is a difference in operating frequency between our design (3 GHz) and simulation (2.88 GHz). Theoretically, we assumed the SSP on the ring have uniform phase constant, but in reality the stubs on the ring are unequal, leading to nonuniform wavenumber of SSP. This is the reason for the frequency shift.

To study the resonance modes, we used a near-field scanning set-up to characterize the E_z-field distributions in the x-y plane 1 mm above the antenna at the operating frequency, which are depicted in Fig. 6. It is observed that all the patterns present the whispering gallery resonances. Moreover, the azimuthal order of the WGMs m range from 9, 10, and 11, which are in accord with our prediction in Table I. We proceed to investigate the azimuthal component of electric fields E_φ of the radiated wave. The setup of the measurement is shown in Fig. 7. An open-end waveguide is used as the receiver, which moves in the plane and stores the electric fields data. Actually, there is mode dispersion occurs when the vortex beam transmits through the turbulent medium. In order to minimize the influence of medium and ensure that the fields reflect the performance of the antenna itself, a short propagation distance is a better choice for OAM mode analysis. Therefore, we set the distance between the receiver and our OAM antenna as

$$R = 0.62\sqrt{\frac{D^3}{\lambda}} \approx 100 \ mm \qquad (12)$$

, which is taken to be inner boundary of radiating near-field region [43].

Firstly, the electric fields distributions of x- and y-polarization in the plane 100 mm above the antenna are simulated and stored. Then we convert electric fields in cartesian coordinates to cylindrical coordinates. The simulated phase and field E_φ distributions under different varactors values are shown in Fig. 8 (a) and (b). The waves exhibit spiral phase in the case of 0.23 pF and 0.36 pF, while no OAM with 0.3 pF. The phase changes along the azimuth direction of -2π, 0, and 2π are achieved under c_v = 0.23 pF, 0.3 pF, and 0.36 pF, respectively. It is evident that the emitted field from our antenna carries OAM of l = −1, 0, and 1 at each of the varactor values, respectively. In addition, the measured phase and instant field

distributions of E_φ on the cut plane of 540×510 mm^2 at 100 mm above the proposed device under different reverse voltages are also presented in Fig. 8 (c) and (d). Good agreement between experimental and simulated results validates our vortex antenna design.

The purity of OAM modes is quantitatively calculated by using the Fourier transform. Since the azimuth angle φ is a periodic function, its Fourier conjugate is the OAM spectrum [44]. The OAM spectrum can be written as

$$A_l = \frac{1}{2\pi}\int_0^{2\pi} \psi(\varphi)exp(-jl\varphi)d\varphi \tag{12}$$

where $\psi(\varphi)$ is the sampling phase. Fig. 9 shows the purity weight of the OAM with $c_v = 0.23$ pF, 0.3 pF, and 0.36 pF, respectively. All the generated vertex beams have excellent purity, as high as 90%. Meanwhile, the azimuthal electric field component E_φ can be expressed as the combination of left-hand circularly polarized (LHCP) and right-hand circularly polarized (RHCP) components. Therefore, the E_φ VVBs of topological charge l can be decomposed into two scalar vortices given by

$$E_\varphi = E_0 e^{-jl\varphi}\hat{\varphi} = -\frac{j}{2}\big[-E_0(\hat{x}-j\hat{y})e^{-j(l-1)\varphi} \\ + E_0(\hat{x}+j\hat{y})e^{-j(l+1)\varphi}\big] \tag{13}$$

It is also observed that the LHCP vortex beam carry OAM of $l + 1$, while RHCP vortex beam carry OAM of $l - 1$. Hence, our design can combine VVBs and scalar vortex beams.

Fig. 10 presents the simulated LHCP and RHCP far-field patterns and phase distributions with varying varactor values. As expected, the LHCP far-field pattern is a pencil-like beam with $c_v = 0.23$ pF, while diverging radiation patterns with 0.3 pF and 0.36 pF. As illustrated in Fig. 10(b), the LHCP far field have spiral phase change equal to 0, 2π, and 4π with 0.23 pF, 0.3 pF, and 0.36 pF, which correspond to the OAM modes $l = 0$, 1, and 2, respectively. The RHCP patterns are in stark contrast with LHCP. When the varactor is 0.23 pF, and 0.3 pF, the far-filed patterns are hollow, as shown in Fig. 10(c). A focused radiation pattern is corresponding to emitted beam with 0.36 pF. The RHCP phase patterns have spiral arms equal to 2, 1, and 0, corresponding topological of -2, -1, and 0, respectively. These far-field results agree well with the predictions. Therefore, our antenna can also generate the tunable scalar vortex wave with the reconfigurable OAM modes at fixed frequency.
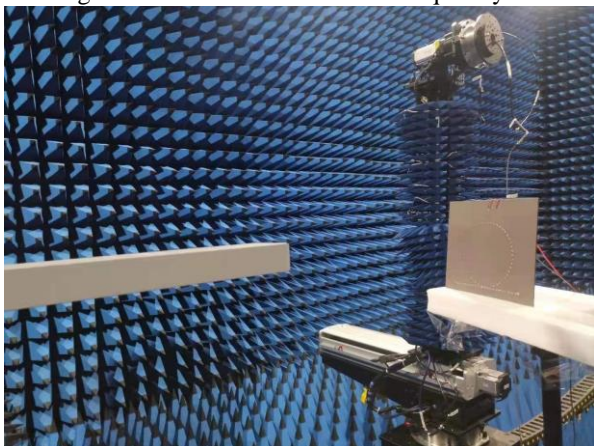

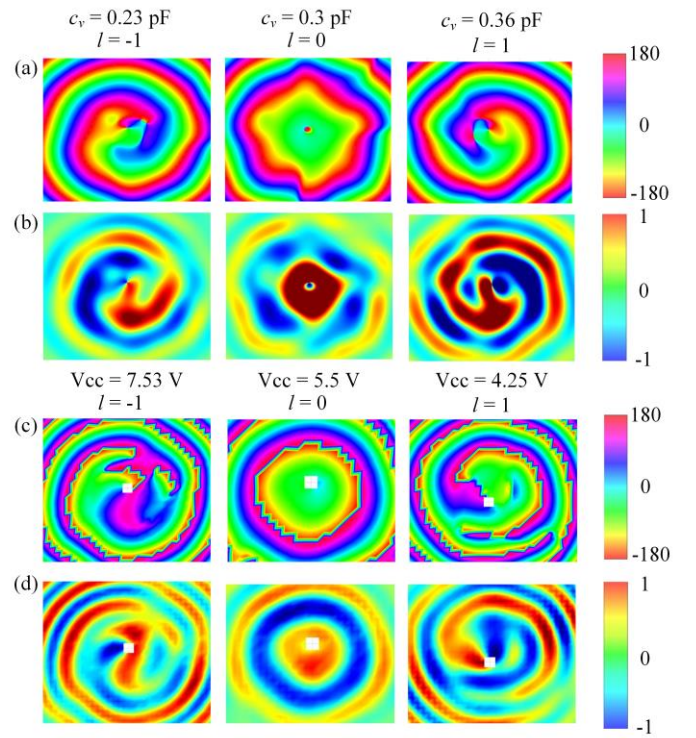Fig. 7 Experimental setup in an anechoic chamber.

Fig. 8 Simulated (a) phase and (b) instant electric field distribution of emitted wave with the azimuthal polarization at different varactor values. Measured (c) phase and (d) instant electric field distribution of emitted wave with the azimuthal polarization under different voltage.
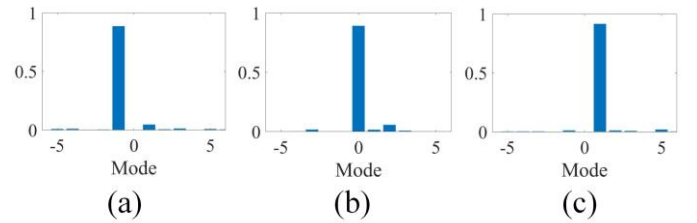

Fig.9 OAM purity weight for the simulated results. (a) $c_v = 0.23$ pF (b) $c_v = 0.3$ pF (c) $c_v = 0.36$ pF.

To further verify the radiation performance of our design, the radiation efficiencies are simulated, which are 63%, 28%, and 50% with 0.23 pF, 0.3 pF, and 0.36 pF, respectively. Here, the radiation efficiencies suffer from the effects of the parasitic resistance of the varactor diode M46H120. The use of less stubs and varactors could mitigate this problem; however, reducing the stub numbers would decrease the quality of the phase front as well as the OAM state purity. Here, we made the tradeoff between the radiation efficiency and the purity. The optimum stub numbers are set as 50.

Fig. 11 provides the comparison of simulated and measured far-field patterns in yoz cut plane. The red lines indicate the simulated results with different varactor values 0.23 pF, 0.3 pF and 0.36 pF. The blue symbol lines denote the measured far-fields with different reverse voltage, which are 7.53 V, 5.5 V and 4.25 V, respectively. The simulated and measured patterns exhibit a relatively good agreement. The radiation patterns are slight asymmetry, especially at theta = 90° and 270°. The principal reason for this performance is the feedline influence. As expected, LHCP wave with 0.23 pF presents an ordinary

beam while others have amplitude null in the center. For RHCP, pencil-like beam with 0.36 pF originates from topological charge of zero, whereas others do not.
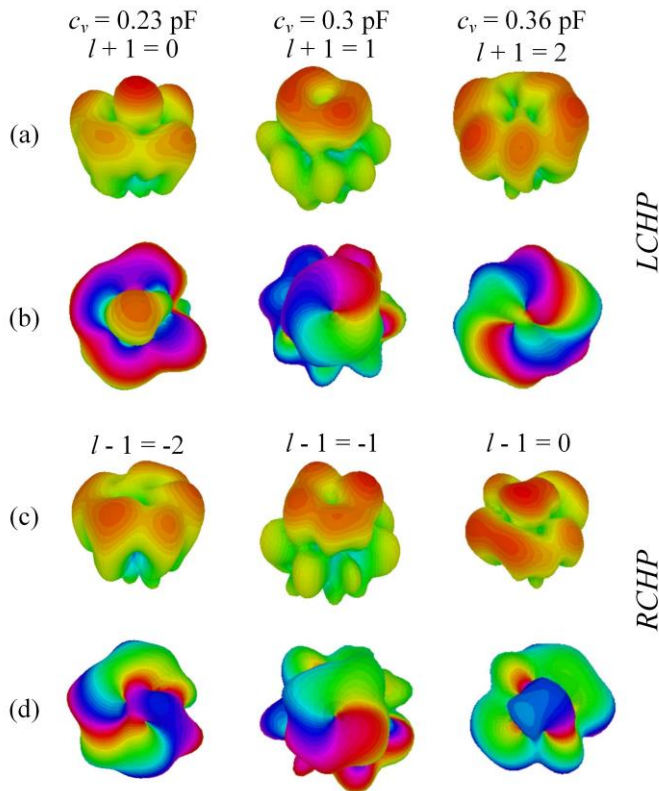

Fig. 10 Numerically calculated far-field (a) radiation patterns and (b) phase patterns of the emitted LHCP beams with different varactor values. Numerically calculated far-field (c) radiation patterns and (d) phase patterns of the emitted RHCP beams with different varactor values.

V. CONCLUSION

VVBs with different OAM modes are observed at fixed frequency utilizing the tunable surface impedance of the ring, which can be obtained by changing the varactor values through DC bias voltage. Simulation and measurement results fully confirm the theoretical prediction. The OAM modes of $l = -1$, 0, and 1 appear with 0.23 pF (7.53 V), 0.3 pF (5.5 V), and 0.36 pF (4.25 V), respectively. Moreover, LHCP and RHCP scalar vortex beams carrying OAM have also been investigated. We envision that the proposed antenna would find important applications in wireless communication and imaging.
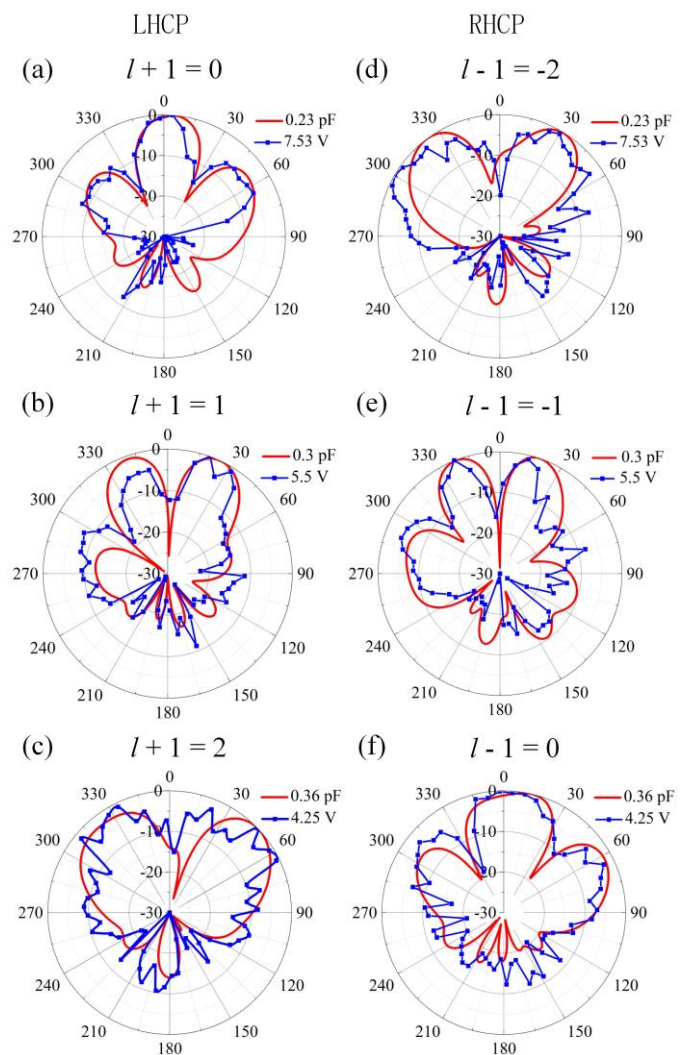

Fig. 11 Measured and simulated far-field 2D radiation patterns of (a) LHCP and (b) RHCP

REFERENCES

[1] F. Tamburini, E. Mari, A. Sponselli, B. Thidé, A. Bianchini, and F. Romanato, "Encoding many channels on the same frequency through radio vorticity: first experimental test," *New J. Phys.*, vol. 14, no. 3, p. 033001, Mar. 2012.

[2] L. Allen, M. W. Beijersbergen, R. J. C. Spreeuw, and J. P. Woerdman, "Orbital angular momentum of light and the transformation of Laguerre-Gaussian laser modes," *Phys. Rev. A*, vol. 45, no. 11, pp. 8185–8189, Jun. 1992.

[3] Q. Zhan, "Cylindrical vector beams: from mathematical concepts to applications," *Adv. Opt. Photon.*, vol. 1, no. 1, pp. 1–57, Jan. 2009.

[4] S. Quabis, R. Dorn, M. Eberler, O. Glöckl, and G. Leuchs, "Focusing light to a tighter spot" *Opt. Commun.*, vol. 179, no. 1, pp. 1–7, May 2000.

[5] R. Dorn, S. Quabis, and G. Leuchs, "Sharper Focus for a Radially Polarized Light Beam," *Phys. Rev. Lett.*, vol. 91, no. 23, p. 233901, Dec. 2003.

[6] R. Chen, K. Agarwal, C. J. R. Sheppard, and X. Chen, "Imaging using cylindrical vector beams in a high-numerical-aperture microscopy system," *Opt. Lett.*, vol. 38, no. 16, pp. 3111–3114, Aug. 2013.

[7] S. Segawa, Y. Kozawa, and S. Sato, "Demonstration of subtraction imaging in confocal microscopy with vector beams," *Opt. Lett.*, vol. 39, no. 15, pp. 4529–4532, Aug. 2014.

[8] B. J. Roxworthy and K. C. Toussaint, "Optical trapping with π-phase cylindrical vector beams," *New J. Phys.*, vol. 12, no. 7, p. 073012, Jul. 2010.

This article has been accepted for publication in a future issue of this journal, but has not been fully edited. Content may change prior to final publication. Citation information: DOI 10.1109/TAP.2022.3161487, IEEE Transactions on Antennas and Propagation

> REPLACE THIS LINE WITH YOUR PAPER IDENTIFICATION NUMBER (DOUBLE-CLICK HERE TO EDIT) <   8

[9]   Y. Kozawa and S. Sato, "Optical trapping of micrometer-sized dielectric particles by cylindrical vector beams," *Opt. Express*, vol. 18, no. 10, pp. 10828–10833, May 2010.

[10] D. G. Grier, "A revolution in optical manipulation," *Nature*, vol. 424, no. 6950, pp. 810–816, Aug. 2003.

[11] B. Ndagano, R. Brüning, M. McLaren, M. Duparré, and A. Forbes, "Fiber propagation of vector modes," *Opt. Express,* vol. 23, no. 13, pp. 17330–17336, Jun. 2015.

[12] B. Ndagano, I. Nape, M. A. Cox, C. Rosales-Guzman, and A. Forbes, "Creation and Detection of Vector Vortex Modes for Classical and Quantum Communication," *J. Lightwave Technol.,* vol. 36, no. 2, pp. 292–301, Jan. 2018.

[13] R. Chen, J. Wang, X. Zhang, J. Yao, H. Ming, and A. Wang, "Fiber-based mode converter for generating optical vortex beams," *Opto-Electron. Adv.*, vol. 1, no. 7, pp. 180003-180003–7, Aug. 2018.

[14] W. Cheng, J. W. Haus, and Q. Zhan, "Propagation of vector vortex beams through a turbulent atmosphere," *Opt. Express,* vol. 17, no. 20, pp. 17829–17836, Sep. 2009.

[15] F. Cardano, E. Karimi, S. Slussarenko, L. Marrucci, C. de Lisio, and E. Santamato, "Polarization pattern of vector vortex beams generated by q-plates with different topological charges," *Appl. Opt.,* vol. 51, no. 10, pp. C1–C6, Apr. 2012.

[16] H. Chen, J. Hao, B.-F. Zhang, J. Xu, J. Ding, and H.-T. Wang, "Generation of vector beam with space-variant distribution of both polarization and phase," *Opt. Lett.,* vol. 36, no. 16, pp. 3179–3181, Aug. 2011.

[17] A. Niv, G. Biener, V. Kleiner, and E. Hasman, "Manipulation of the Pancharatnam phase in vectorial vortices," *Opt. Express,* vol. 14, no. 10, pp. 4208–4220, May 2006.

[18] J. Liu *et al.*, "Generation of arbitrary cylindrical vector vortex beams with cross-polarized modulation," *Results in Phys.*, vol. 19, p. 103455, Dec. 2020.

[19] Y. Zhang, J. Gao, and X. Yang, "Spatial variation of vector vortex beams with plasmonic metasurfaces," *Sci. Rep.*, vol. 9, no. 1, p. 9969, Jul. 2019.

[20] X. Yi *et al.*, "Generation of cylindrical vector vortex beams by two cascaded metasurfaces," *Opt. Express,* vol. 22, no. 14, pp. 17207–17215, Jul. 2014.

[21] Y. Bao, J. Ni, and C.-W. Qiu, "A Minimalist Single-Layer Metasurface for Arbitrary and Full Control of Vector Vortex Beams," *Adv. Mater.*, vol. 32, no. 6, p. 1905659, 2020.

[22] F. Yue, D. Wen, J. Xin, B. D. Gerardot, J. Li, and X. Chen, "Vector Vortex Beam Generation with a Single Plasmonic Metasurface," *ACS Photon.*, vol. 3, no. 9, pp. 1558–1563, Sep. 2016.

[23] Z. H. Jiang and B. Gao, "Millimeter-Wave Transmit-Arrays for Vector Vortex Beam Generation," in *2021 15th European Conference on Antennas and Propagation (EuCAP)*, Dusseldorf, Germany, Mar. 2021, pp. 1–4.

[24] M. Akram, X. Bai, R. Jin, G. Vandenbosch, M. Premaratne, and W. Zhu. "Photon spin Hall effect-based ultra-thin transmissive metasurface for efficient generation of OAM waves." *IEEE Trans. Antennas Propaga.*, vol. 67, no. 7, pp. 4650-4658, 2019.

[25] G. Su *et al.*, "Demonstration of microwave plasmonic-like vortices with tunable topological charges by a single metaparticle," *Appl. Phys. Lett.*, vol. 118, no. 24, p. 241106, Jun. 2021.

[26] H. Feng, L. Ye, Y. Zhang, W. Li, H. Chen, and Q. H. Liu, "Bidirectional multi-mode microwave vortex beam generation enabled by spoof surface plasmon polaritons," *Appl. Phys. Lett.*, vol. 117, no. 24, p. 241601, Dec. 2020.

[27] H. Su *et al.*, "Efficient Generation of Microwave Plasmonic Vortices via a Single Deep-Subwavelength Meta-Particle," *Laser Photon. Rev.*, vol. 12, no. 9, p. 1800010, Sep. 2018.

[28] J. Y. Yin, J. Ren, L. Zhang, H. Li, and T. J. Cui, "Microwave Vortex-Beam Emitter Based on Spoof Surface Plasmon Polaritons," *Laser Photon. Rev.*, vol. 12, no. 3, p. 1600316, Mar. 2018.

[29] Z. Liao *et al.*, "Microwave-Vortex-Beam Generation Based on Spoof-Plasmon Ring Resonators," *Phys. Rev. Appl.*, vol. 13, no. 5, p. 054013, May 2020.

[30] H. Xu, H. Liu, X. Ling, Y. Sun, and F. Yuan, "Broadband Vortex Beam Generation Using Multimode Pancharatnam–Berry Metasurface," *IEEE Trans. Antennas Propag.*, vol. 65, no. 12, pp. 7378–7382, Dec. 2017.

[31] S. Zheng, X. Hui, X. Jin, H. Chi, and X. Zhang, "Transmission Characteristics of a Twisted Radio Wave Based on Circular Traveling-Wave Antenna," *IEEE Trans. Antennas Propag.*, vol. 63, no. 4, pp. 1530–1536, Apr. 2015.

[32] Q. Liu, Z. N. Chen, Y. Liu, F. Li, Y. Chen, and Z. Mo, "Circular Polarization and Mode Reconfigurable Wideband Orbital Angular Momentum Patch Array Antenna," *IEEE Trans. Antennas Propag.*, vol. 66, no. 4, pp. 1796–1804, Apr. 2018.

[33] Y. Gong *et al.*, "Generation and Transmission of OAM-Carrying Vortex Beams Using Circular Antenna Array," *IEEE Trans. Antennas Propagt.*, vol. 65, no. 6, pp. 2940–2949, Jun. 2017.

[34] H. Shi *et al.*, "Generation of Multiple Modes Microwave Vortex Beams Using Active Metasurface," *IEEE Antennas Wireless Propag. Lett.*, vol. 18, no. 1, pp. 59–63, Jan. 2019.

[35] X. Bai, F. Kong, Y. Sun, G. Wang, J. Qian, X. Li, A. Cao, C. He, X. Liang, R. Jin, and W. Zhu., "High-efficiency transmissive programmable metasurface for multimode OAM generation." *Advanced Optical Materials,* vol. 8, no. 17, pp. 2000570, 2020.

[36] H. C. Zhang, P. H. He, X. Gao, W. X. Tang, and T. J. Cui, "Pass-band reconfigurable spoof surface plasmon polaritons," *J. Phys.: Condens. Matter*, vol. 30, no. 13, p. 134004, 2018.

[37] S. A. Maier, *Plasmonics: fundamentals and applications*. New York: Springer, 2007.

[38] X. Zhang *et al.*, "A Spoof Surface Plasmon Transmission Line Loaded with Varactors and Short-Circuit Stubs and Its Application in Wilkinson Power Dividers," *Adv. Mater Techn.*, vol. 3, no. 6, p. 1800046, 2018.

[39] Pozar. D. M, *Microwave Engineering*. Publishing House of Elec, 2004.

[40] A. Oliner, and A. Hessel. "Guided waves on sinusoidally-modulated reactance surfaces," *IRE Trans. Antennas Propaga.*, vol. 7, no. 5, pp. 201-208, 1959.

[41] M. Wang, H. F. Ma, H. C. Zhang, W. X. Tang, X. R. Zhang, and T. J. Cui, "Frequency-Fixed Beam-Scanning Leaky-Wave Antenna Using Electronically Controllable Corrugated Microstrip Line," *IEEE Trans. Antennas Propag.*, vol. 66, no. 9, pp. 4449–4457, Sep. 2018.

[42] C. A. Balanis, *Antenna theory: analysis and design*, 3rd ed. Hoboken, NJ: John Wiley, 2005.

[43] Y. Guang, L. Zhang, W. Li, and Q. Liu. "Orbital angular momentum spectrum of antenna vortex beam based on loop integration," *AIP Advances*, vol. 11, no. 11, pp. 115204, 2021.

[44] E. Yao, S. Franke-Arnold, J. Courtial, S. Barnett, and M. Padgett, "Fourier relationship between angular position and optical orbital angular momentum," *Opt. Exp.* vol. 14, no. 20, pp. 9071, 2006.

Zhen Liao (M'20) received the Ph.D. degree from Southeast University, Nanjing, China, in 2017. Since 2017, he joined the College of Electromagnetics and Information Engineering, Hangzhou Dianzi University, where he is currently an associate professor. From Nov. 2018 to Jun. 2020, he joined the Department of Electrical, Electronic, Northeastern University, Boston, U.S.A., as a visiting scientist. His current research interests include metamaterials, antennas, and microwave circuits.

Yanziyi Che is currently working towards the master degree in Hangzhou Dianzi University, Zhejiang, China. His current research interests include spoof surface plasmon polarities and antennas.

Leilei Liu (S'03–M'09) received the B.Sc. and Ph.D. degrees in electromagnetic and microwave technology from Southeast University, Nanjing, China, in 2003 and 2009, respectively. She studied in Linnaeus University, Kalmar, Sweden, as an international student in 2004. Since 2009, she has been with Nanjing University of Posts and Telecommunications, Nanjing, China, as an associate professor. From 2015 to 2016, she was with the Poly-Grames Research Center, Montreal, Canada, as a visiting scholar. Her current research interests include antennas, spoof surface plasmon polaritons and microwave circuits.

Bai Cao Pan received the Ph.D. degree in electrical engineering from Southeast University, Nanjing, China in 2018.

He joined the College of Electromagnetics and Information Engineering, Hangzhou Dianzi University, where he is currently an associate professor. His research interests include engineered electromagnetic structures, metamaterials, spoof surface plasmon polaritons, antennas, and microwave circuits.
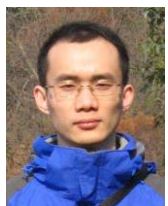
Bengeng Cai was born in Zhejiang, China. He received the B.S. degree and the M.S. degree in physics from Zhejiang University, Hangzhou, China, in 2002 and 2005 respectively, and Ph.D. degree in radio engineering from Southeast University, Nanjing, China, in 2017.

Since 2017, he has been a Lecturer with the faculty of School of Electronics and Information, Hangzhou Dianzi University. Since 2020, he has been a Post-Doctoral Fellow with the Poly-Grames Research Center, Polytechnique Montréal, University of Montreal, Montreal, QC, Canada. His research interests include metasurface and leaky-wave antennas.

JiaNan Zhou received the M.D. degree from Hangzhou Dianzi University, Hangzhou, China, in 2021. Since 2021, he has been an engineer in Xiaomi Communications Co., Ltd. His current research interests include spoof surface plasmon and antennas.

Guo Qing Luo (M'08-SM'18) received the B.S. degree from the China University of Geosciences, Wuhan, China, in 2000, the M.S. degree from Northwest Polytechnical University, Xi'an, China, in 2003, and the Ph.D. degree from Southeast University, Nanjing, China, in 2007.

Since 2007, he has been a Lecturer with the faculty of School of Electronics and Information, Hangzhou Dianzi University, Hangzhou, China, and was promoted to Professor in 2011.

From Oct. 2013 to Oct. 2014, he joined the Department of Electrical, Electronic and Computer Engineering, Heriot-Watt University, Edinburgh, U.K., as a Research Associate, where he was involved in developing low profile antennas for UAV applications. He has authored or co-authored over 140 technical papers in refereed journals and conferences and holds over 30 patents. His current research interests include RF, microwave and mm-wave passive devices, antennas, and frequency selective surfaces.

Dr. Luo was a recipient of the CST University Publication Award in 2007, the National Excellent Doctoral Dissertation of China in 2009, the National Natural Science Award (2nd class) of China in 2016, and the Natural Science Award (2nd class) of Zhejiang Province, China in 2021. He is a Fellow of the Chinese Institute of Electronics, and the Chair of IEEE Microwave Theory and Techniques Society Hangzhou Chapter. He has served as TPC chairs of 2021 National Conference on Antennas (NCANT 2021), 2021 International Conference on Microwave and Millimeter Wave Technology (ICMMT 2021), 2018 UK-Europe-China Workshop on Millimeter Waves and Terahertz Technologies (UCMMT 2018), and 2017 National Conference on Microwave and Millimeter Waves (NCMMW 2017), and Organizing Committee Chair of 2011 China-Japan Joint Microwave Conference (CJMW 2011). He also serves as guest editors for some technical journals including IET Microw., Antennas & Propag., and Electronics, and as reviewers for many technical journals, including the IEEE Trans. Antennas Propag., IEEE Trans. Microw. Theory Tech., IEEE Antennas Wireless Propag. Lett., IEEE Microw. Wireless Comp. Lett., and IEEE Transactions on Circuits and Systems etc.

Yongmin Liu obtained his Ph.D. from the University of California, Berkeley in 2009. He joined the faculty of Northeastern University at Boston in fall 2012 and is currently an associate professor in the Department of Mechanical & Industrial Engineering and the Department of Electrical & Computer Engineering. His research interests include nano optics, nanoscale materials, plasmonics, metamaterials, and nano-optomechanics. He has authored and coauthored more than 100 journal papers. He was a recipient of NSF CAREER Award (2017), SPIE Defense and Commercial Sensing Rising Researcher (2016), and 3M Non-Tenured Faculty Award (2016).